NASA TM X-54,065

NASA TM X-54,065

EFFECT OF AXIAL FLOW ON THE BEHAVIOR OF THE WALL-CONSTRICTED ARC

By Howard A. Stine, Velvin R. Watson
and Charles E. Shepard

Thermo- and Gas-Dynamics Division
NASA, Ames Research Center
Moffett Field, Calif.

Presented to the AGARD Specialists' Meeting
on Arc Heaters and MHD Accelerators
for Aerodynamic Purposes
Rhode-Saint-Genese,
Belgium
September 21-23, 1964

ABSTRACT

An experimental and theoretical study of the interaction between an electric arc and a coaxial flow of gas has been carried out in a range of size, enthalpy level, and pressure level where radiation heat loss is a noticeable portion of the total loss from the system. Numerical calculations have been performed and have been compared with earlier analytic calculations and also with the experimental results. Although differences in the detailed behavior of the gas flow-arc interaction are predicted by the two theoretical methods, the integrated behavior as deduced by either of the theoretical methods is essentially the same. Moreover, this integrated behavior is in substantial agreement with the experimental results, at least insofar as predictions of buildup of energy flux is concerned.

FIGURE LEGENDS

Fig. 1.- Instrumentation for constricted-arc supersonic jet, 1.27-cm-diameter throat.

Fig. 2.- Performance map for constricted-arc supersonic jet.

Fig. 3.- Variation of enthalpy scaling parameter with length scaling parameter with nitrogen.

Fig. 4.- Effect of arc current on constrictor heat loss at various nitrogen flow rates.

Fig. 5.- Effect of arc current on power input to arc at various nitrogen flow rates.

Fig. 6.- Effect of arc current on average enthalpy in nitrogen.

Fig. 7.- Effect of arc current on stagnation pressure at various nitrogen flow rates.

Fig. 8.- Calculated distributions of various quantities through 1.27-cm-diameter constrictor at a current of 770 A and air flow rate of 0.0016 kg/sec. (a) Variation of enthalpy with length and radius. (b) Variation of specific mass flux with length and radius. (c) Variation of energy flux with length and radius. (d) Variation of momentum flux with length and radius. (e) Variation of velocity with length and radius.

Fig. 9.- Comparison of numerical calculations and analytical calculations with various experimental measurements at a current of 770 A and air flow of 0.0016 kg/sec. (a) Variation of center-line enthalpy with axial distance. (b) Variation of space average enthalpy with axial distance. (c) Variation of mass average enthalpy with axial distance.

(d) Variation of pressure and ratio of average enthalpy to center-line enthalpy with axial distance. (e) Variation of wall heat flux with axial distance. (f) Variation of voltage gradient with axial distance.

Fig. 10.- Measured radial distributions of heat flux and impact pressure at nozzle exit for air flow of 0.005 kg/sec. (a) Heat flux and impact pressure profiles at power input of 215 kw. (b) Heat flux and impact pressure profiles at power input of 285 kw. (c) Heat flux and impact pressure profiles at power input of 350 kw.

SYMBOLS

A	area
C_c	conversion constant
d	diameter
E	voltage gradient
H	average enthalpy
h	enthalpy
I	current
k	thermal conductivity
l	length
p	pressure
Q	power loss
$\dot{q}$	wall heat-transfer rate
r	radial distance from axis
T	temperature
u	axial velocity
v	radial velocity
$\dot{w}$	weight flow rate
z	axial distance
θ	angular coordinate about axis
μ	viscosity
ρ	density
σ	electrical conductivity
φ	thermal conductivity potential, $\int k dT$

EFFECT OF AXIAL FLOW ON THE BEHAVIOR OF THE WALL-CONSTRICTED ARC

By Howard A. Stine, Velvin R. Watson,
and Charles E. Shepard

National Aeronautics and Space Administration
Ames Research Center
Moffett Field, Calif.

1. INTRODUCTION

During the past three years, a considerable effort, both theoretical and experimental, has been made to understand the manner in which a flow of gas becomes heated as it travels along the axis of a wall-constricted, direct-current electric arc. As a result of a number of studies (1-7), it may be stated that at least a qualitative understanding of the process is now in hand, and that one may predict with a reasonable degree of assurance the performance of small-diameter constricted-arc-jet devices which operate at pressure levels near 1 atmosphere. However, little is understood of the behavior of large-diameter constricted-arc jets at higher pressure and enthalpy levels where radiation transport is an appreciable source of energy loss. The purpose of this paper is to discuss from a theoretical point of view, and from an experimental point of view insofar as it is presently possible, the behavior of the wall-constricted arc in the presence of flow along the axis under conditions of sufficiently great pressure, enthalpy, and size that the radiation energy losses have a noticeable effect on constrictor behavior.

2. APPARATUS

The experimental measurements to be discussed have been carried out in the apparatus illustrated in Fig. 1. This device and another similar device of one-half size have been described in detail elsewhere (1,7). In brief, the apparatus illustrated consists of a DeLaval nozzle having a throat diameter of 1.27 centimeters and having electrodes so arranged that a direct-current electric arc can be established between the high-pressure plenum chamber on the left and the exit of the supersonic nozzle on the right.

The upstream electrode is made of tungsten, and is operated as the cathode. To protect it from attacks of chemically active gases, the tungsten cathode is bathed in an atmosphere either of argon or nitrogen. Much larger quantities of any gas desired, such as air, nitrogen, and CO_2-nitrogen mixtures, can be admitted into the plenum chamber just downstream of the cathode shroud. The main flow of gas can be admitted either with a tangential component of velocity, or swirl, or with negligible vorticity. Because the flow is aerodynamically choked near the exit of the cylindrical throat, or constrictor tube, the static pressure decrease along the length amounts to about one-half of the stagnation pressure.

The downstream electrode, or anode, operates in the region of supersonic flow. It consists of 24 elements, each having a 2-ohm ballast resistor. The current flow to each element can thus be limited to values of 50 amperes or less, even though total currents as great as 1200 amperes can be accommodated. The supersonic jet exit, just downstream of the anode, is equipped with probes and traversing equipment for obtaining radial profiles of impact pressure and heat-transfer rate.

for the 1.27-cm-diameter constrictor. At pressures of about 1 atmosphere, one predicts a maximum average energy content of approximately 4×10^8 J/kg. However, as the pressure is raised to approximately 10 atmospheres, the enthalpy capability falls by a factor of approximately 10 because of the increased wall heat load due to radiation.

Also shown on the figure are calculated radial distributions of energy content for an indefinitely long constrictor at selected values of pressure. At 1 atmosphere, for example, the shape of the profile is very nearly that of the zero order Bessel function of the first kind (3), the center-line value of enthalpy being 2.3 times as great as the average enthalpy. As the pressure increases, the profiles become flatter and broader. At 10 atmospheres a constant distribution of enthalpy with radius exists over more than 50 percent of the cross section, and the center-line enthalpy is less than twice the average.

It can be seen that operation with the apparatus of Fig. 1 has been achieved through the pressure range from 1 to 3 atmospheres where radiation heat loss constitutes a rapidly increasing portion of the total. By virtue of its larger diameter alone, the larger constrictor tube encounters a radiative heat load about twice that of the smaller unit. Accordingly, one might expect to detect experimentally the influence of radiation heat loss. This point will be discussed later.

4. EXPERIMENTAL RESULTS WITH NEGLIGIBLE RADIATION LOSS

At pressure of 1 atmosphere or less, where conduction is the dominant heat-loss mechanism, the performance of the device having the smaller throat, has been well documented (7). The results of a large number of tests with

The constrictor tube is constructed from a number of copper rings, each separated from its neighbor by means of boron nitride spacers. The spacers serve as electric insulation so that the arc-column voltage gradient can be supported by the metal wall. Each of the rings is provided with a cooling passage, through which water is circulated at high velocity.

Instrumentation is provided to monitor total current, voltage gradient, total heat loss, mass flow, and pressure.

3. OPERATING RANGE

Constricted-arc supersonic jets have been operated with nitrogen gas at the levels of enthalpy (determined by means of power balance) and pressure illustrated on Fig. 2, wherein enthalpy in joules per kilogram is plotted against pressure in atmospheres. As shown by the shaded area, the smaller device has been operated over a stagnation pressure range from 0.3 to 1.0 atmosphere at average enthalpy levels up to 10^8 J/kg. Somewhat higher pressure levels have been reached with the larger unit at approximately the same values of average enthalpy with both air and nitrogen.

It has been fairly well established that the maximum enthalpy which can be contained within an indefinitely long cylindrical constrictor is limited by the heat-transfer rate which can be maintained across the wall at the downstream end. When the walls are metal, and when the coolant is water, the maximum heat-transfer rate which can be accommodated is about 10 kw/sq cm (2). With this heat-transfer rate as a constraint, it is possible to calculate as a function of pressure the maximum value of average enthalpy that can be contained (2,5). Figure 2 displays such a calculation

nitrogen gas show the behavior illustrated by the open symbols on Fig. 3. This figure is a plot of enthalpy scaling parameter, $Hd/2I$, versus length scaling parameter, $l/\dot{w}$. The grouping of variables comprising the ordinate and abscissa (see symbols) are those that emerge from the arc-column theory (3), and should collapse the data onto a single curve. As can be observed from a comparison of the data points with the theoretical curve indicated on the figure, agreement is fairly good. As has been shown (1), the ordinate and abscissa can be generalized to allow for correlation of data from any gas. Because of the several idealizations contained in the theory (3), better agreement with experiment should not be expected. The theory, however, has the virtue of predicting in a simple way length, diameter, current, voltage mass flow, heat loss, and average enthalpy relationships that are valuable for the purpose of making engineering estimates of performance.

5. EXPERIMENTAL RESULTS WITH APPRECIABLE RADIATION LOSS

The data for the 1.27-cm-diameter constrictor, shown by the solid symbols on Fig. 3, tend to lie systematically below the theory of (3), in which radiation loss is neglected. Such a trend might be expected as a function of diameter, because the radiation component of the heat loss from the larger constrictor would be approximately 4 times that from the smaller constrictor at identical values of enthalpy and pressure. Moreover, the conductive component of the heat loss would decrease less rapidly with increasing diameter than would be predicted by the theory (3) because of the tendency for the increasing radiation flux to broaden the radial enthalpy profile. Thus, departures from the simple proportionality between enthalpy and current

embodied in the enthalpy scaling parameter of Fig. 3 would be expected as radiation heat loss becomes an increasing fraction of the total.

A simple test to evaluate these departures of the constrictor behavior from the predictions of theory (3) consists in measuring heat loss as a function of electric current at fixed values of mass flow. Because the mass flow is fixed, the constrictor enthalpy will rise with current and, hence, pressure will increase. Thus, it would be expected that the radiation heat loss would increase, by virtue of increases both in enthalpy and in pressure.

Figure 4 shows the results of such a test with nitrogen gas in the constricted-arc supersonic jet of Fig. 1. Total heat loss is plotted as a function of arc current at various fixed values of mass flow. The theory (3) predicts that the total heat loss is due to conduction only, and increases exactly linearly with arc current at fixed mass flow. As can be observed from Fig. 4, however, very appreciable departures from linearity occur at currents greater than about 400 amperes. It can thus be reasoned that radiation heat loss becomes relatively more important at high current and/or that the heat-conduction theory (3) does not adequately describe constrictor behavior at high current.

Tests have also been performed to determine the effects of variable-current operation at fixed flow rate on power input, average enthalpy, and plenum pressure. Results of these tests are shown in Figs. 5, 6, and 7. Again, according to theory (3), power input and average enthalpy increase exactly linearly with increasing arc current. Figure 5 indicates, however, that the power delivered to the constricted arc increases with current at a greater rate than linearly, but not as rapidly as does the

heat loss shown in Fig. 4. Consequently, as Fig. 6 shows, average enthalpy increases with current at a somewhat slower rate than linearly. The dashed straight line on Fig. 6 represents the variation of average enthalpy with current that would be predicted by theory (3) at a mass flow of 0.005 kg/sec. Although, as is apparent from Fig. 7, the stagnation pressure rises by a modest factor as current is raised from 150 to 800 amperes, a relatively large increase in radiation can be expected because of the strong dependence of radiation power density on pressure level (2).

6. THEORETICAL PREDICTIONS USING NUMERICAL METHODS

The question arises as to whether or not the observed behavior of the constricted-arc supersonic jet, as attested by Figs. 4, 5, 6, and 7, can be predicted by numerical computations. Calculations have been performed that include in the energy equation the loss of energy by means of radiation, and the radial convection of energy, in addition to the terms considered in the analysis of (3). Moreover, the equation for conservation of the axial component of momentum has been included to yield velocity and momentum-flux profiles. Furthermore, a set of equations designed to explore the behavior of the flow through an off-axis arc column has been studied. These calculations, in which nonlinear values of gas properties are introduced, are compared both with experimental data and with certain analytic results (3) in which gas property relationships were linearized. The new calculations were carried out by a finite-difference technique on a high-speed electronic-digital computer.

The two systems of differential equations that were studied are as follows:

(1) For axisymmetric conditions without swirl in the constrictor tube:

$$\left.\begin{aligned} &\frac{\rho u\,\partial h}{\partial z} + \frac{\rho v\,\partial h}{\partial r} = \frac{C_c I^2 \sigma}{\left[\int_A \sigma dA\right]^2} + \frac{u\,dp}{dz} + \frac{1}{r}\frac{\partial \varphi}{\partial r} + \frac{\partial^2 \varphi}{\partial r^2} - \text{Radiation} \\ &\frac{\rho u\,\partial u}{\partial z} + \frac{\rho v\,\partial u}{\partial r} = -\frac{dp}{dz} + \frac{1}{r}\frac{\partial}{\partial r}\left(r\mu\frac{\partial u}{\partial r}\right) \\ &\int_A \rho u dA = \dot{w} \end{aligned}\right\} \quad (1)$$

(2) For flow through the off-axis arc without swirl:

$$\left.\begin{aligned} &\frac{\rho u\,\partial h}{\partial z} = \frac{C_c I^2 \sigma}{\left[\int_A \sigma dA\right]^2} + \frac{u\,dp}{dz} + \frac{1}{r}\frac{\partial \varphi}{\partial r} + \frac{\partial^2 \varphi}{\partial r^2} + \frac{1}{r^2}\frac{\partial^2 \varphi}{\partial \theta^2} - \text{Radiation} \\ &\frac{\rho u\,\partial u}{\partial z} = -\frac{dp}{dz} + \frac{1}{r}\frac{\partial}{\partial r}\left(r\mu\frac{\partial u}{\partial r}\right) + \frac{1}{r^2}\frac{\partial}{\partial \theta}\left(\mu\frac{\partial u}{\partial \theta}\right) \\ &\int_A \rho u dA = \dot{w} \end{aligned}\right\} \quad (2)$$

Values of the dependent variables ρ, μ, φ, σ, and radiation transport were tabulated as functions of p and h by synthesis of available published information for the gases air and nitrogen considered to be in local thermodynamic equilibrium. The various sources (8-12) from which the needed information was taken are presented in table 1.

Solutions to finite-difference forms of the sets of Eqs. (1) and (2) were obtained by a process of forward marching along the constrictor, using total current, I, total mass flow, $\dot{w}$, and diameter, d, as parameters. Various initial radial distributions of enthalpy at the constrictor inlet

were arbitrarily selected, and the constrictor wall temperature was held at an arbitrary fixed value. Integration was usually, but not necessarily, terminated at axial distances, l, at which calculations indicated the flow became aerodynamically choked.

7. RESULTS OF NUMERICAL CALCULATIONS

Equations (2) were solved for arbitrary symmetrical and asymmetrical distributions of enthalpy at the inlet of the 1.27-cm-diameter tube. The solutions show that, in cases where the current is sufficiently great and the mass flow sufficiently small, the asymmetrical distribution rapidly becomes symmetrical. For current greater than 300 amperes and mass flows less than 0.01 kg/sec, the distribution became symmetrical in an axial distance of less than three diameters. Thus the interaction between the flow and the discharge appears to be stable with respect to deviation from axial symmetry.

One solution of Eqs. (1) for axisymmetric flow of air is illustrated in Fig. 8. This figure shows distributions of various quantities with respect to radius and length of the 1.27-cm-diameter constrictor at a current of 770 amperes and a flow rate of 0.0016 kg/sec. The wall enthalpy was maintained at a value of 5.75×10^5 J/kg. The shape of the initial enthalpy profile with which the integration was started at the inlet is shown on Fig. 8(a). Also shown is the manner in which the enthalpy profile changes with the radius and length as the flow is followed along the constrictor tube axis. As can be seen from the figure, the initial profile was assumed to fill just one-half the diameter of the tube. As the flow

proceeds along the axis, it can be observed that the enthalpy at first rises sharply to a peak about one-quarter of a diameter downstream from the tube entrance. At this point it can also be observed that the profile has spread rapidly until the wall is reached. Thereafter the enthalpy at the center line decreases rapidly, approaches a constant value which persists along the remainder of the length of the constrictor tube, and exhibits a shape remarkably constant with axial distance.

Figure 8(b) shows the variation of specific mass flux, ρu, with length and radius for the same current and flow rate parameters. At the tube entrance initial conditions were selected for which very little flow actually passes through the core, most of it bypassing the arc column and crowding against the wall. As the arc column radius grows with length, however, and expands toward the wall, more and more of the flow is ingested into the column and the variation of mass flux with radius approaches a fairly uniform value. At an axial distance of approximately one-quarter meter, the profile is almost uniform with radius except for vestigial peaks very near the tube wall.

Figure 8(c) shows the corresponding variation of energy flux, ρuh, with length and radius. For the parameters chosen, the curve shows that the buildup of this parameter is very rapid and that the energy flux becomes approximately constant with length beyond an axial distance of one-tenth of a meter. The energy flux is an important quantity because the radially averaged value of this term is what one determines by means of a heat balance in an experimental study of arc-jet behavior. The experimental data are usually reduced by the strategem of dividing the

measured average energy flux by the total mass flow to produce an average value of enthalpy. Thus the average energy flux is proportional to the enthalpy that one would deduce from heat-balance measurements.

Figure 8(d) illustrates the variation of momentum flux, ρu^2, with length and radius. Momentum flux, of course, is proportional to the impact pressure that one would measure at the tube exit. As can be observed, the center-line value of momentum flux continually increases throughout the length of the constrictor. It rises, however, much more rapidly at the inlet than it does farther downstream. Comparison at fixed axial distance of the variation with radius of energy flux (Fig. 8(c)) with a corresponding curve of momentum flux reveals a pronounced lack of similarity, the momentum-flux profile being the broader of the two.

Finally, Fig. 8(e) illustrates the variation of velocity with length and radius. These profiles exhibit a behavior quite similar to those of the momentum flux. A rapid increase evident at the inlet is followed by a somewhat smaller increase with distance throughout the majority of the length of the constrictor tube.

8. COMPARISON OF NUMERICAL RESULTS WITH EXPERIMENT AND ANALYTICAL SOLUTIONS

Selected trends derived from the curves illustrated on Fig. 8 have been compared with various corresponding trends from the analytical solutions of Ref. 3 and with air data from the apparatus of Fig. 1. Figure 9 shows a number of such comparisons. Again, these correspond to a current of 770 amperes at an air mass flow of 1.6×10^{-3} kg/sec.

Figure 9(a) illustrates the variation of center-line enthalpy with axial distance. As was evident on Fig. 8(a), the numerical solution indicates that the enthalpy on the center line rises extremely rapidly near the entrance to a very high value and decays to a constant value which persists throughout the majority of the constrictor. The corresponding variation of center-line enthalpy, as deduced from the theory (3) does not agree at all at small axial distance, and overestimates the enthalpy value at the exit. It should be noted, however, that the enthalpy values, as deduced from either of the theoretical solutions, differ by only about 25 percent at the outlet of the constrictor tube, even though the detailed behavior at the inlet is grossly different because of the assumed differences in starting conditions and because of the idealizations in the theory (3).

Figure 9(b) illustrates the variation of space-average enthalpy, $1/A\int h dA$, with axial distance. Here it can be seen that the numerically determined distribution of enthalpy rises extremely rapidly to a high value in the first one-tenth meter of the tube length. Thereafter it increases slowly with length. Again, the theory (3) illustrates the exponential behavior implicit in its formulation, and enthalpy does not achieve an asymptotic limit throughout the one-quarter meter length of the constrictor tube. However, at the tube exit the difference between the two predictions is smaller, being in this case not more than about 12 percent.

Figure 9(c) shows the variation of mass-average enthalpy, $1/\dot{w}\int \rho u h dA$, with axial distance as calculated by the two methods. As was previously mentioned, this quantity corresponds to that determined experimentally by heat-balance measurements. Differences between values of mass-average

enthalpy and space-average enthalpy (Fig. 9(b)) at a given axial distance reflect the effects of departures from uniformity of the radial distribution of specific mass flux, ρu, the two averages being identical according to (3). Here, opportunity exists to effect a comparison with experimental data. Values determined with the apparatus of Fig. 1, shown on Fig. 9(c), lie between the calculated curves, and are about 5 percent greater than the numerically calculated values. The experimentally determined value of enthalpy at the constrictor inlet was 24.7×10^6 J/kg. When the data were placed on the figure, the constrictor entrance was arbitrarily considered to begin at the axial distance where the numerically calculated enthalpy was also 24.7×10^6 J/kg.

Figure 9(d) illustrates, first, the variation of pressure with axial distance and shows that the pressure falls more or less linearly by a factor of approximately 2 along the length of the constrictor. All other things being equal, radiation heat loss should therefore decrease with length. The other curves shown on figure 9(d) depict the ratio of average enthalpy to center-line enthalpy, as a function of axial distance. Again the numerical calculations and the theory (3) are in poor agreement near the constrictor inlet, but the agreement becomes somewhat better near the downstream end.

Figure 9(e) shows the variation of heat loss to the wall with axial distance. Two curves derived from the present numerical calculations are illustrated. The uppermost curve represents the total heat-transfer rate to the wall whereas the lowermost curve represents that portion of the total, as calculated by the numerical method, which is due to thermal radiation. The distribution of heat-transfer rate with length derived

from the theory (3) is also illustrated. It can be observed that the two methods of calculation are in only qualitative agreement throughout the constrictor length. At the exit, the method of (3) predicts only about two-thirds of the wall heat-transfer rate that one calculates numerically. The average heat flow to the wall, $\pi d \int \dot{q} dz$, as determined by the integration of the theoretical distributions yields 96.2 kw for the numerical solution and 85.2 kw for the analytical solution (3). Both these are less than the experimentally determined value of 114 kw. The calculated heat flow due to radiation amounts to 37.1 kw, close to 40 percent of the calculated total heat loss. Note that very near the constrictor inlet the total heat flux consists only of radiation because, as was shown in connection with the discussion of Fig. 8, the arc column at the inlet does not contact the wall. Moreover, the radiation heat loss, after reaching a maximum near the inlet, where both pressure and enthalpy are highest, decreases somewhat from inlet region to exit as a result of falling pressure.

Finally, Fig. 9(f) illustrates the variation of voltage gradient with axial distance. Here, again, the experimental data available for comparison are shown on the plot. As can be seen, neither of the theories is in complete agreement with the data, although the correct magnitude of the voltage gradient is predicted. The fact that the experimentally determined voltage gradient is greater than either of the calculated voltage gradients over the majority of the constrictor length is consistent with the results that the measured heat loss is greater than the calculated loss but the measured and calculated enthalpies are in substantial agreement. The numerical analysis agrees with the experiment somewhat better than does the analytic theory (3).

In summary, it can be stated that the numerical solutions show in somewhat greater detail than has heretofore been possible the behavior of the wall-constricted arc in the presence of axial flow. The comparison of these numerical solutions with the analytical solutions (3) and with data from tests (in air) of a constricted-arc supersonic jet have been carried out. The comparisons indicate that differences in detail regarding the interaction between the arc column and the flowing gas emerge from the two analyses largely because of differences in conditions assumed to exist at the entrance of the constrictor tube in the respective calculation methods. Nevertheless, there is an over-all agreement as to the value of mass-averaged enthalpy attained at the exit of the constrictor tube. Moreover, the agreement between experiment and either of the theoretical predictions is adequate for the purposes of estimating arc-jet performance.

9. FLOW AT NOZZLE EXIT

Finally, it is of interest to examine the experimentally determined distributions of heat transfer and impact pressure obtained by means of radial surveys with hemispherical probes at the exit plane of the supersonic nozzle. Selected distributions are illustrated on Fig. 10. For all the profiles shown the mass flow of air was constant at 5×10^{-3} kg/sec. Figure 10(a) illustrates stagnation-zone heat-flux and impact-pressure profiles at a relatively modest power input of 215 kw. At this input power level the stagnation pressure in the plenum chamber was approximately 1.4 atmosphere. From a comparison of both parts of Fig. 10(a) the shape of the heat-transfer profile appears to be quite independent of the

shape of the impact-pressure profile. Although the impact pressure shows a relatively flat profile that has a central core of approximately 5-cm diameter, the heat-transfer profile is sharply peaked, and can hardly be considered to have a uniform core at all. This trend continues to be evident at higher power input.

Figures 10(b) for instance, indicate the situation at a power level of 285 kw, and Figs. 10(c), show the corresponding distributions at a power level of 350 kw. It should be remarked that the numerical solutions provide evidence that such behavior would be expected. Figure 8 shows, for example, that the profile of momentum flux, ρu^2, is broader than the profile of energy flux, ρuh. It would thus appear that the numerical analysis as so far formulated predicts the observed tendency for nonsimilar profiles.

10. CONCLUDING REMARKS

The effect of axial flow on the behavior of the wall-constricted arc has been discussed from a theoretical point of view and from an experimental point of view insofar as possible. Differences were exhibited between the observed behavior of a constricted-arc supersonic jet and the analytical theory for constricted-arc columns (3). Somewhat more elaborate calculations by means of numerical methods were described, and some of the results of the numerical calculations were discussed.

Comparisons between the analytical predictions and the presumably more exact numerical solutions reveal differences in detail, but no essential differences in qualitative trends and general behavior for the energy flux distribution. The differences in detail appear most strongly near

the upstream, or inlet end of the constrictor, and are due in large part to the widely different assumed upstream boundary conditions. Near the downstream end both methods of calculation are in fair agreement.

Perhaps the largest difference between the numerical solutions and the analytic calculations can be attributed to the influence of radiation heat loss. High enthalpy, large constrictor size, and high pressure all tend to increase the relative importance of radiation as a loss mechanism as compared to conduction as a loss mechanism. Because radiation interacts in a nonlinear manner with the arc-column flow processes, the total heat loss observed at a given enthalpy can be noticeably different than one would predict by means of a linear superposition of radiation flux with a conductive heat flux deduced under the hypothesis that the arc column did not lose energy by radiation. The constrictor diameter, pressure levels, and enthalpies reached in the apparatus were such that radiation heat loss produced a noticeable effect on the results, although radiation was far from being the dominant source of energy loss.

An interesting lack of similarity between heat-transfer-rate profiles and impact-pressure profiles across the exit of the supersonic jet was experimentally observed, the momentum-flux profiles being much broader than the energy-flux profiles. The numerical calculations indicate that such a trend is to be expected.

REFERENCES

1. Shepard, Charles E., and Watson, Velvin R.: Performance of a Constricted-Arc Discharge in a Supersonic Nozzle. Fifth Biennial Gas Dynamics Symposium, Northwestern University, Evanston, Illinois, Aug. 14-16, 1963.

2. Stine, Howard A.: The Hyperthermal Supersonic Aerodynamic Tunnel. Proceedings of the International Symposium on High Temperature Technology. Stanford Research Institute, Sept. 23, 1963.

3. Stine, Howard A., and Watson, Velvin R.: The Theoretical Enthalpy Distribution of Air in Steady Flow Along the Axis of a Direct-Current Arc. NASA TN D-1331, 1962.

4. Jedlicka, James R., and Stine, Howard A.: Axial Flow Through the Wall-Constricted Direct-Current Arc - Comparison of Theory and Experiment. International Symposium on Plasma Phenomena and Measurements. Sponsored by IEEE, San Diego, Calif., Oct. 29, 1963.

5. Cann, G. L., Harder, R. L., Buhler, R. D., and Moore, R. A.: Basic Performance Limits of Coaxial Arc Gas Heaters. EOS Res. Rep. RR-18, 30 Nov., 1963.

6. John, R. R., et al.: Theoretical and Experimental Investigation of Arc Plasma-Generation Technology. Technical Documentary Rep. ASD-TDR-62-729, Parts I and II, Jan. 1963.

7. Shepard, Charles E., Watson, Velvin R., and Stine, Howard A.: Evaluation of a Constricted-Arc Supersonic Jet. NASA TN D-2066, 1964.

8. Ahtye, Warren F., and Peng, Tzy-Cheng: Approximations for the Thermodynamic and Transport Properties of High Temperature Nitrogen With Shock-Tube Applications. NASA TN D-1303, 1962.

9. Yos, Jerrold M.: Transport Properties of Nitrogen, Hydrogen, Oxygen, and Air to 30,000° K. Research and Advanced Development Division, Avco Corporation, RAD TM 63-7, March 1963.

10. Spitzer, L.: Physics of Fully Ionized Gases. Interscience Pub., Inc., N. Y., 1956.

11. Viegas, John R., and Peng, T. C.: Electrical Conductivity of Ionized Air in Thermodynamic Equilibrium. ARS Jour. vol, 31, no. 5, May 1961, pp. 654-657.

12. Hansen, C. Frederick: Approximations for the Thermodynamic and Transport Properties of High-Temperature Nitrogen With Shock-Tube Applications. NASA TR R-50, 1959.

TABLE I.- SOURCES OF TRANSPORT PROPERTY AND STATE DATA FOR AIR AND NITROGEN

Property	Gas				
	Nitrogen		Air		
h(J/kg)	0 - 7×10^7	7×10^7 - 23×10^7	0 - 3.5×10^7	3.5×10^7 - 5.6×10^7	5.6×10^7 - 23×10^7
ρ	Ref. 8	Ref. 9	Ref. 12	Ref. 9	Ref. 9
k	Ref. 8	Ref. 9	Ref. 12	Ref. 8	Ref. 9
σ	Ref. 9	Ref. 9	Ref. 11	Ref. 9	Ref. 9
μ	Ref. 8	Ref. 10	Ref. 12	Ref. 8	Ref. 10
Radiation	Ref. 9	Ref. 9	Ref. 9	Ref. 9	Ref. 9

Ⓐ Shield gas flowmeter

Ⓑ Main gas flowmeter

Ⓒ Typical water flowmeter

Ⓓ Cathode

Ⓔ Typical cooling water supply manifold

Ⓕ Typical cooling water drain manifold

Ⓖ Typical water-temperature thermopile

Ⓗ Galvanometer

Ⓘ Anode cooling water manifold

Ⓙ Cooling water drain manifold and positive bus

Ⓚ Typical 2 Ω ballast resistor

Ⓛ Typical anode

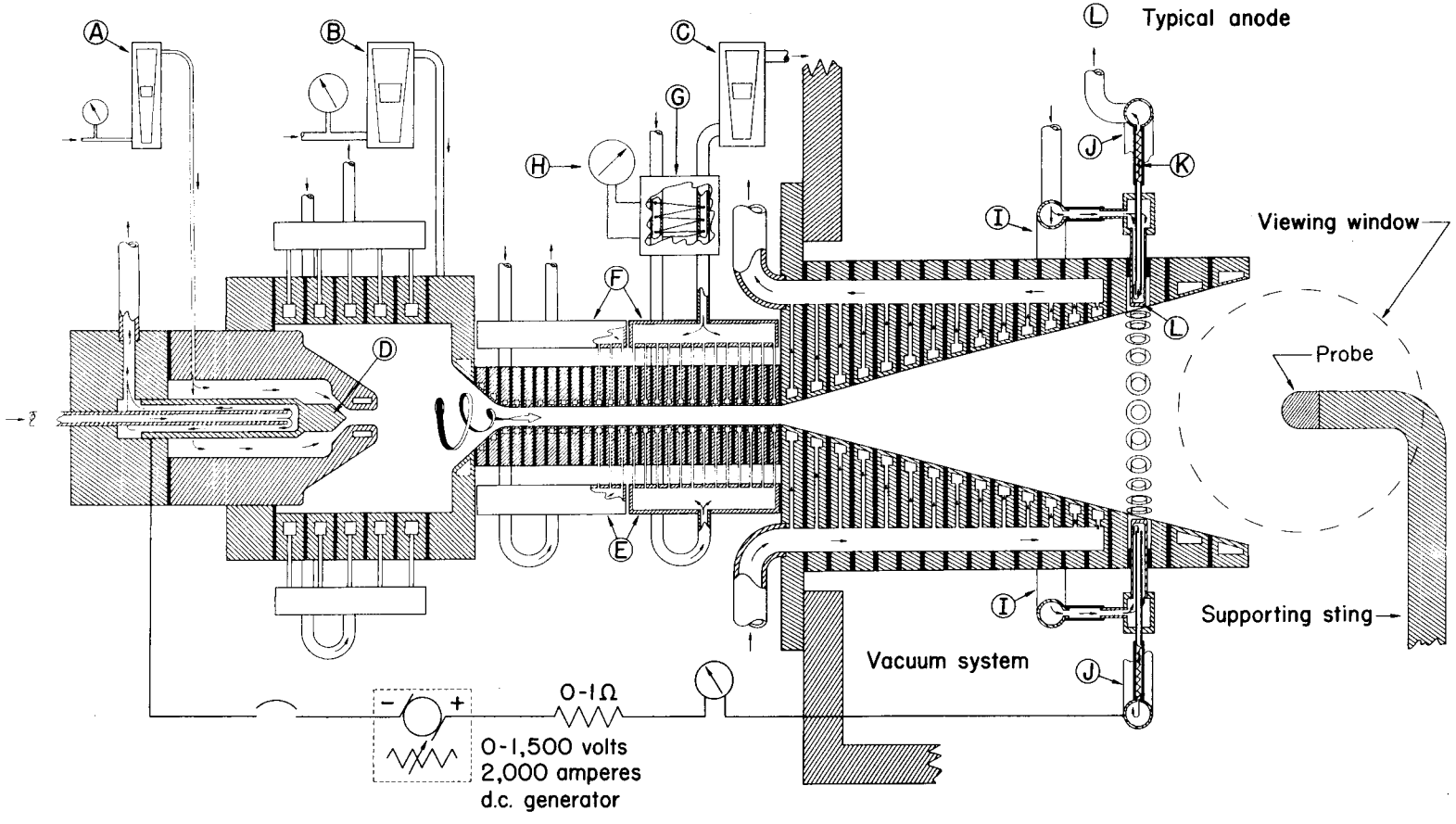

Fig. 1.- Instrumentation for constricted-arc supersonic jet, 1.27-cm-diameter throat.

NATIONAL AERONAUTICS AND SPACE ADMINISTRATION
AMES RESEARCH CENTER, MOFFETT FIELD, CALIFORNIA

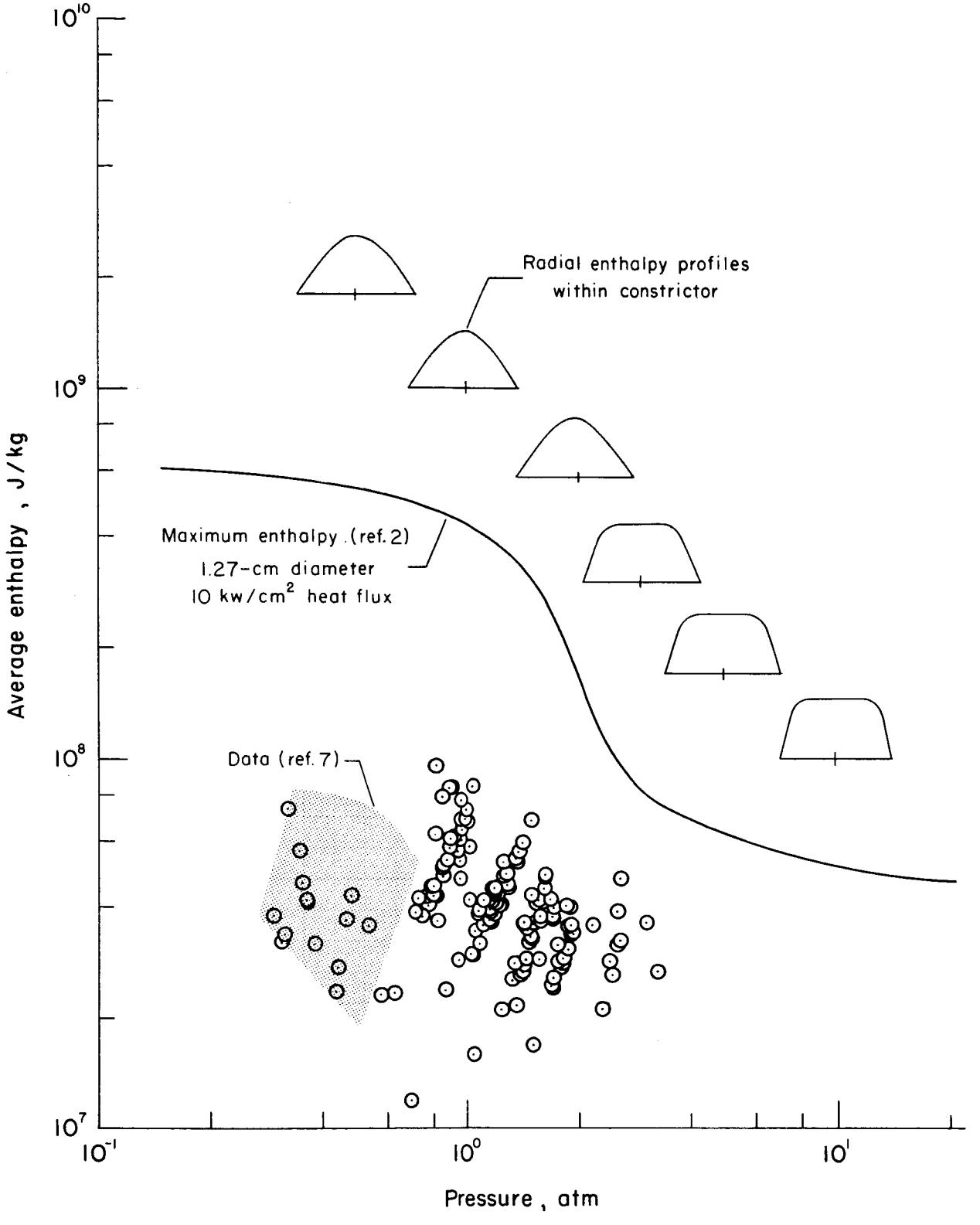

Fig. 2.- Performance map for constricted-arc supersonic jet.

NATIONAL AERONAUTICS AND SPACE ADMINISTRATION
AMES RESEARCH CENTER, MOFFETT FIELD, CALIFORNIA

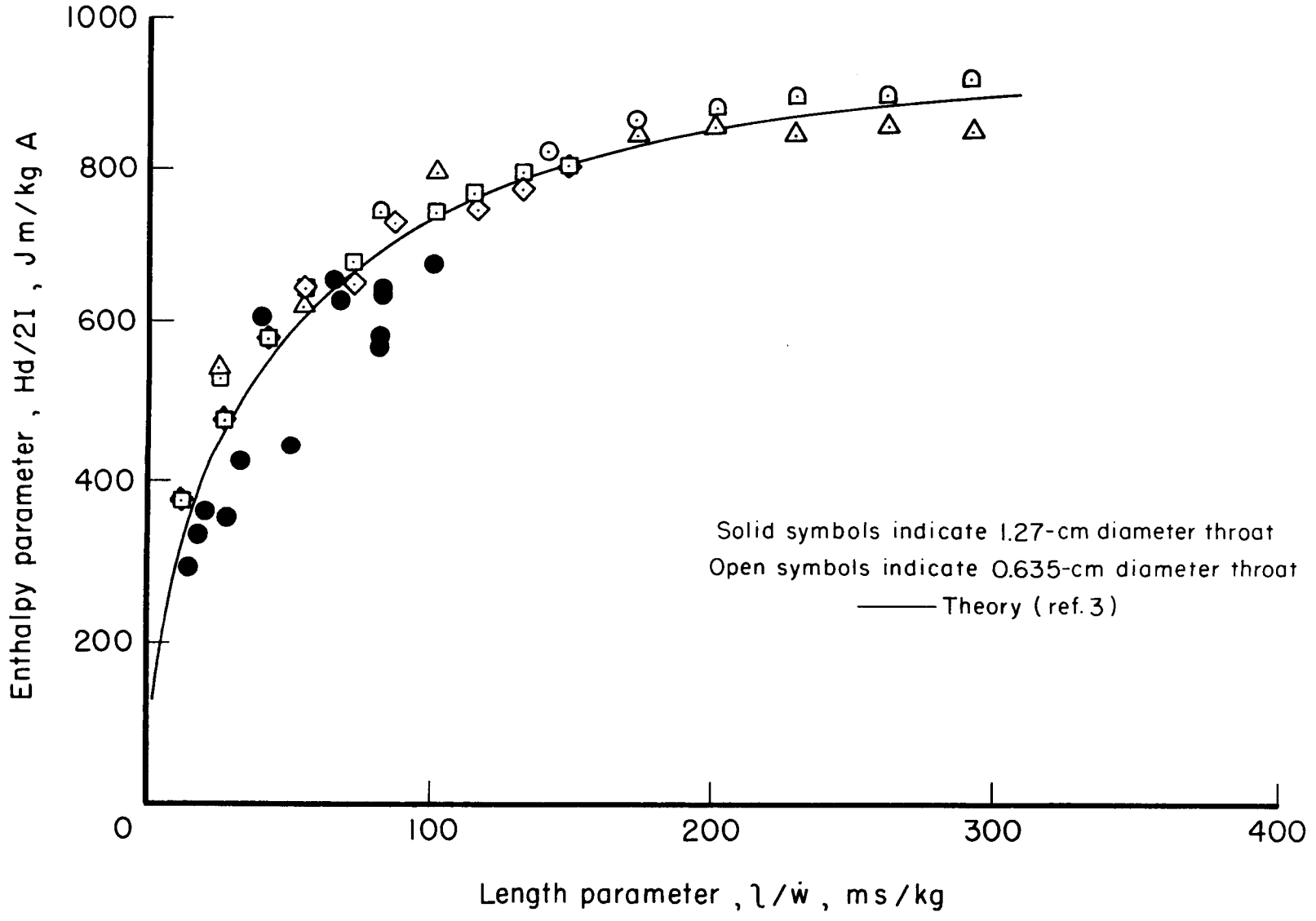

Fig. 3.- Variation of enthalpy scaling parameter with length scaling parameter with nitrogen.

NATIONAL AERONAUTICS AND SPACE ADMINISTRATION
AMES RESEARCH CENTER, MOFFETT FIELD, CALIFORNIA

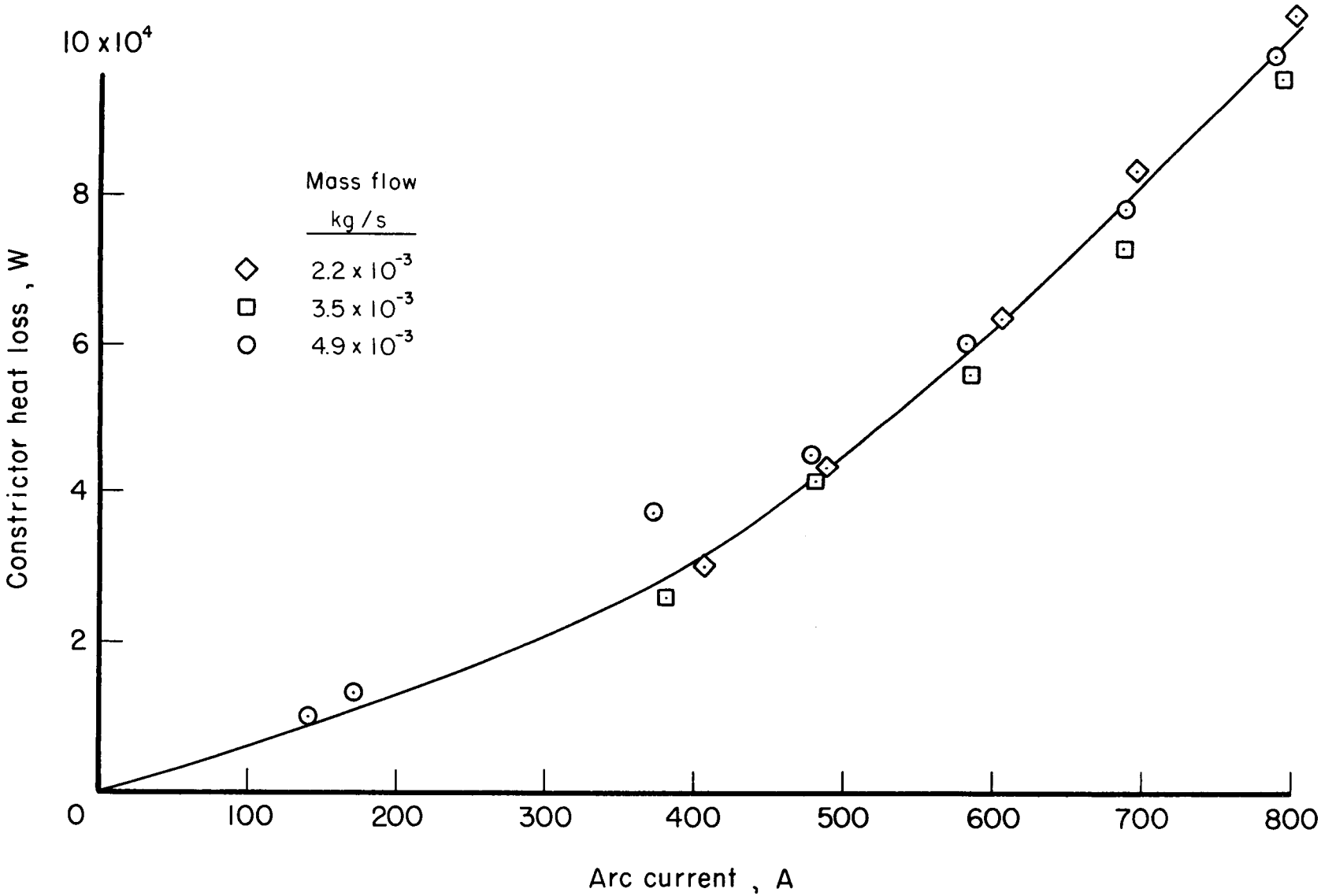

Fig. 4.- Effect of arc current on constrictor heat loss at various nitrogen flow rates.

NATIONAL AERONAUTICS AND SPACE ADMINISTRATION
AMES RESEARCH CENTER, MOFFETT FIELD, CALIFORNIA

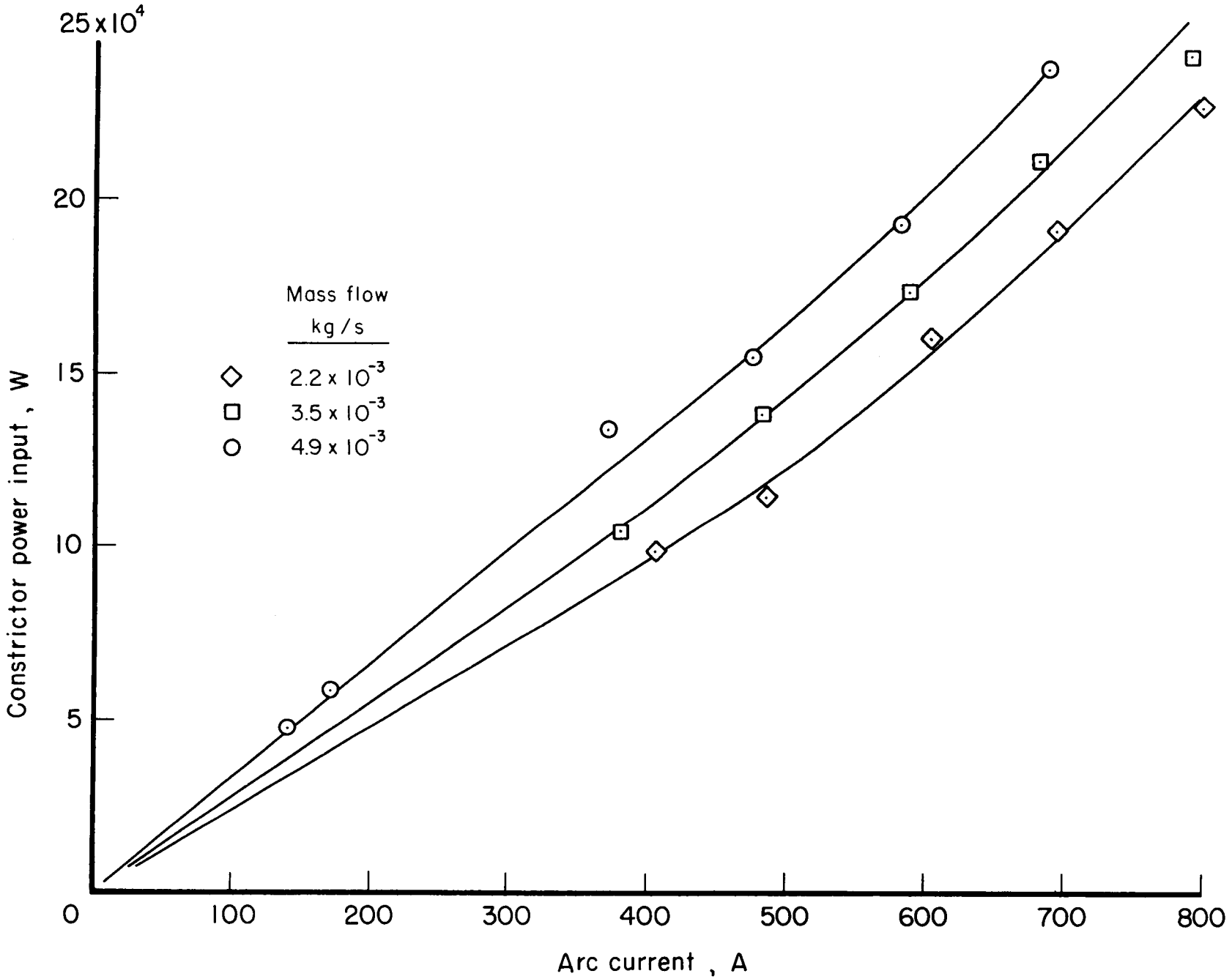

Fig. 5.- Effect of arc current on power input to arc at various nitrogen flow rates.

NATIONAL AERONAUTICS AND SPACE ADMINISTRATION
AMES RESEARCH CENTER, MOFFETT FIELD, CALIFORNIA

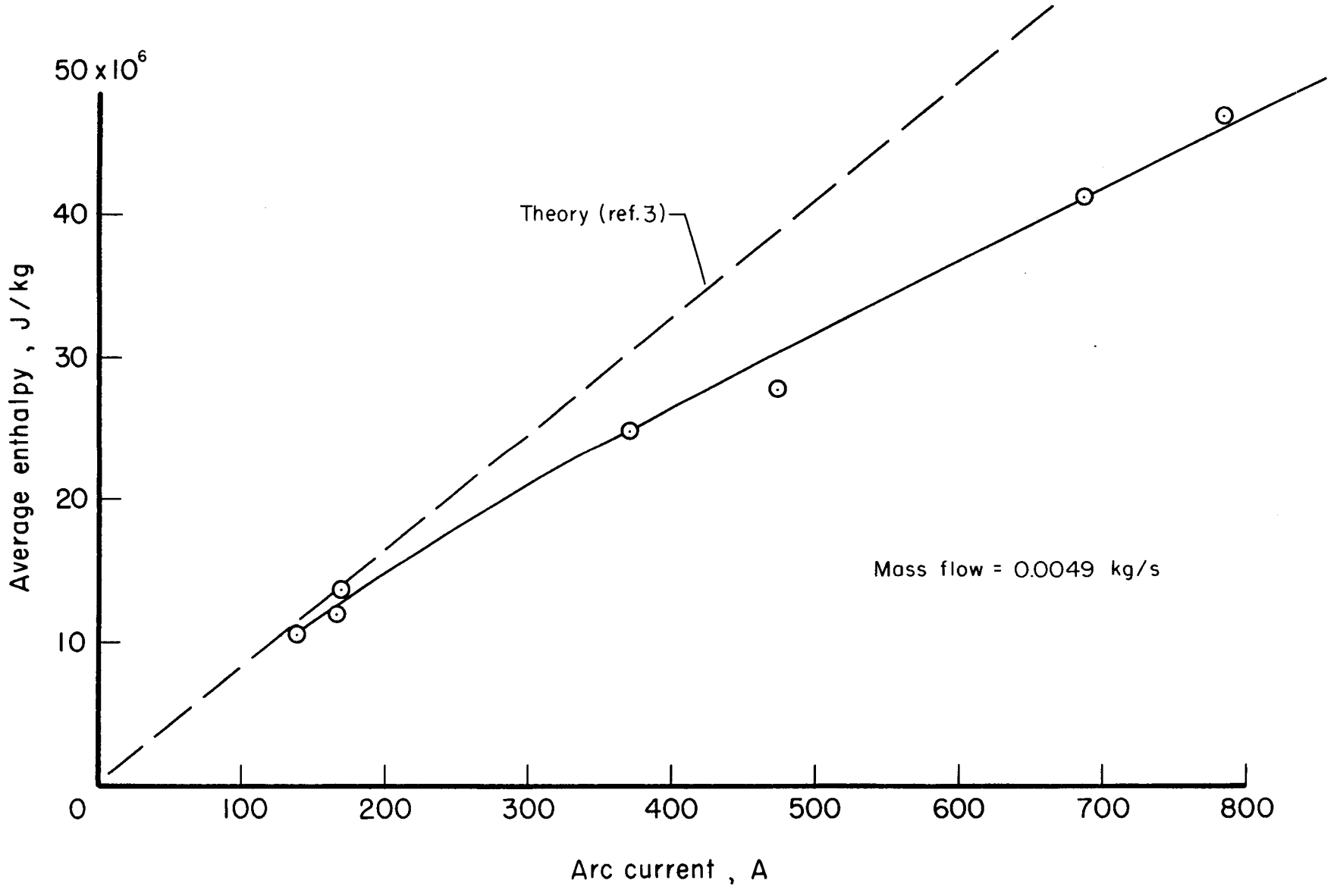

Fig. 6.- Effect of arc current on average enthalpy in nitrogen.

NATIONAL AERONAUTICS AND SPACE ADMINISTRATION
AMES RESEARCH CENTER, MOFFETT FIELD, CALIFORNIA

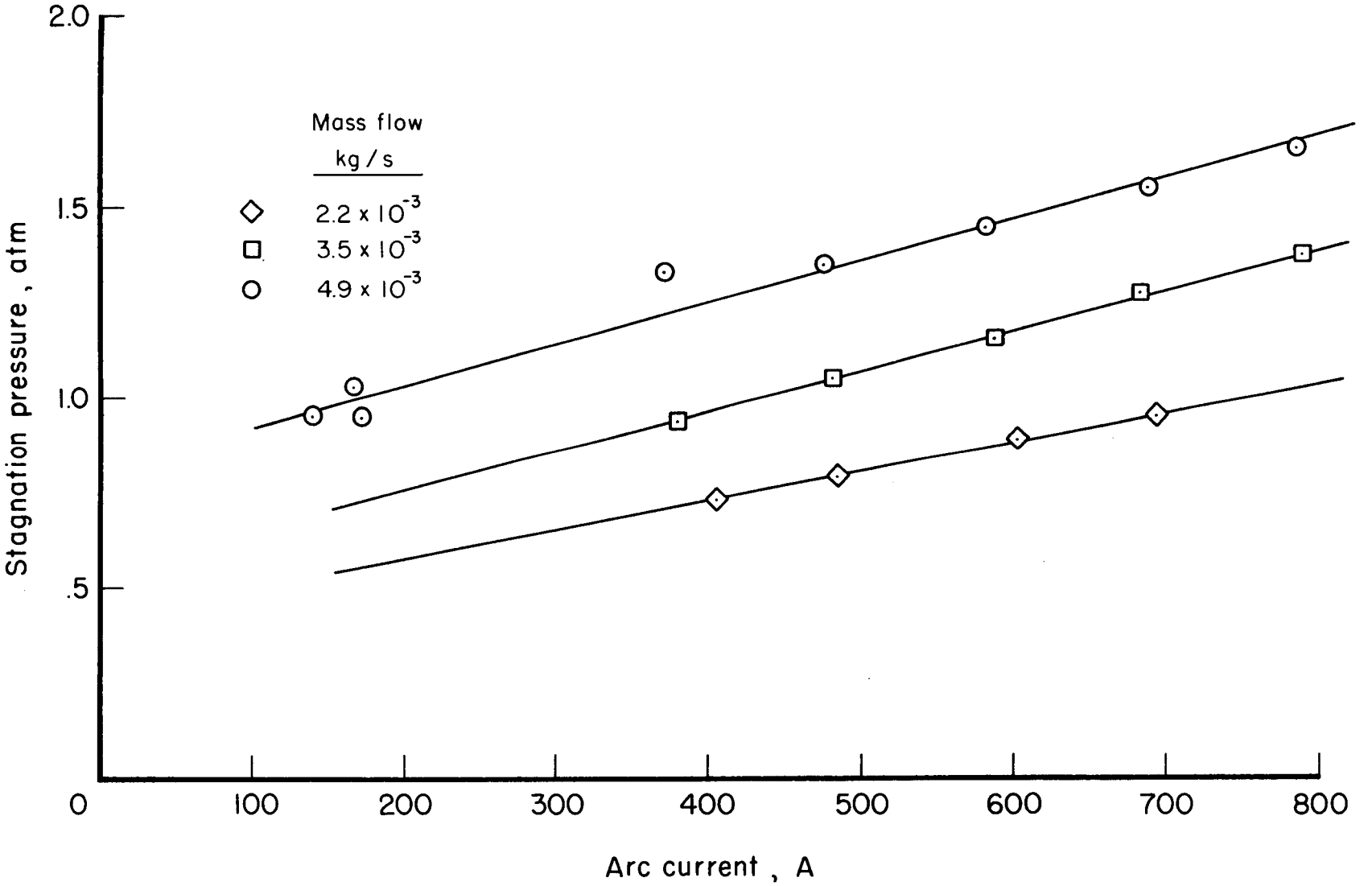

Fig. 7.- Effect of arc current on stagnation pressure at various nitrogen flow rates.

NATIONAL AERONAUTICS AND SPACE ADMINISTRATION
AMES RESEARCH CENTER, MOFFETT FIELD, CALIFORNIA

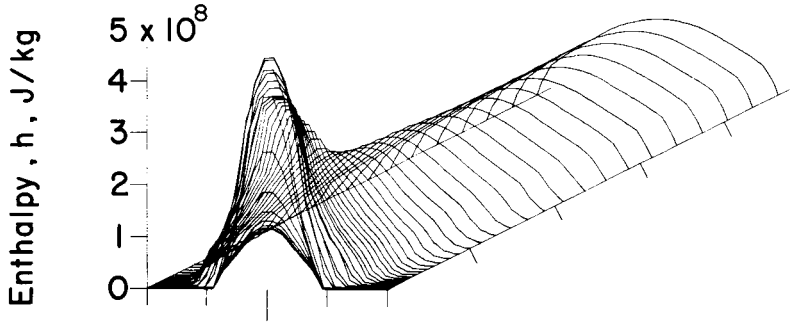

(a) Variation of enthalpy with length and radius.

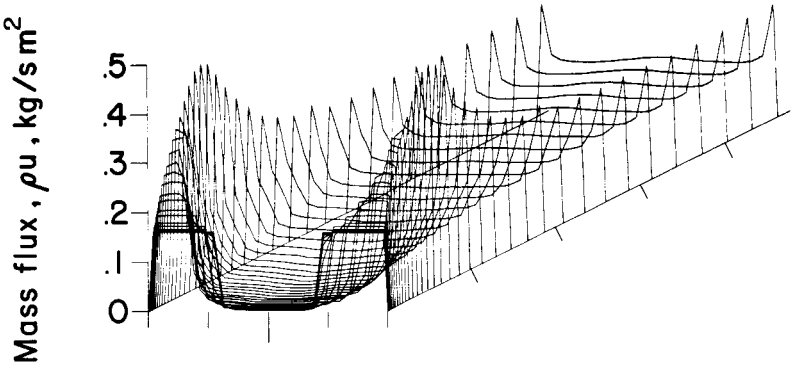

(b) Variation of specific mass flux with length and radius.

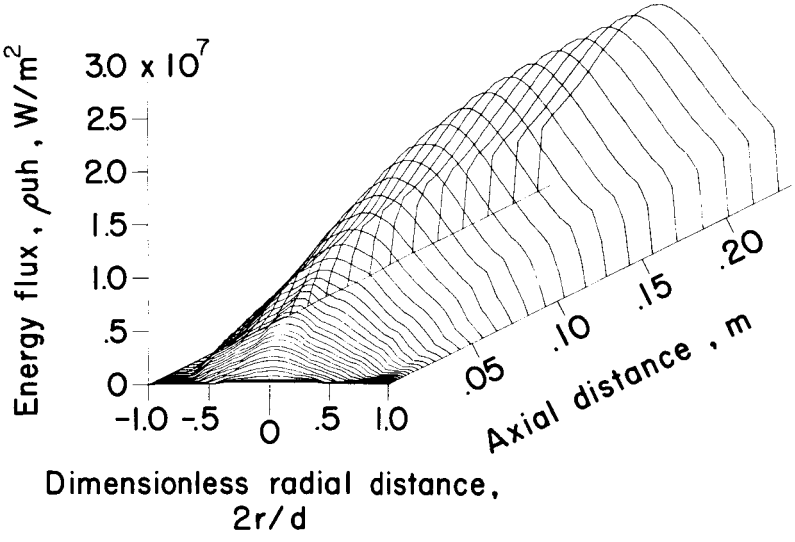

(c) Variation of energy flux with length and radius.

Fig. 8.- Calculated distributions of various quantities through 1.27-cm-diameter constrictor at a current of 770 A and air flow rate of 0.0016 kg/sec.

NATIONAL AERONAUTICS AND SPACE ADMINISTRATION
AMES RESEARCH CENTER, MOFFETT FIELD, CALIFORNIA

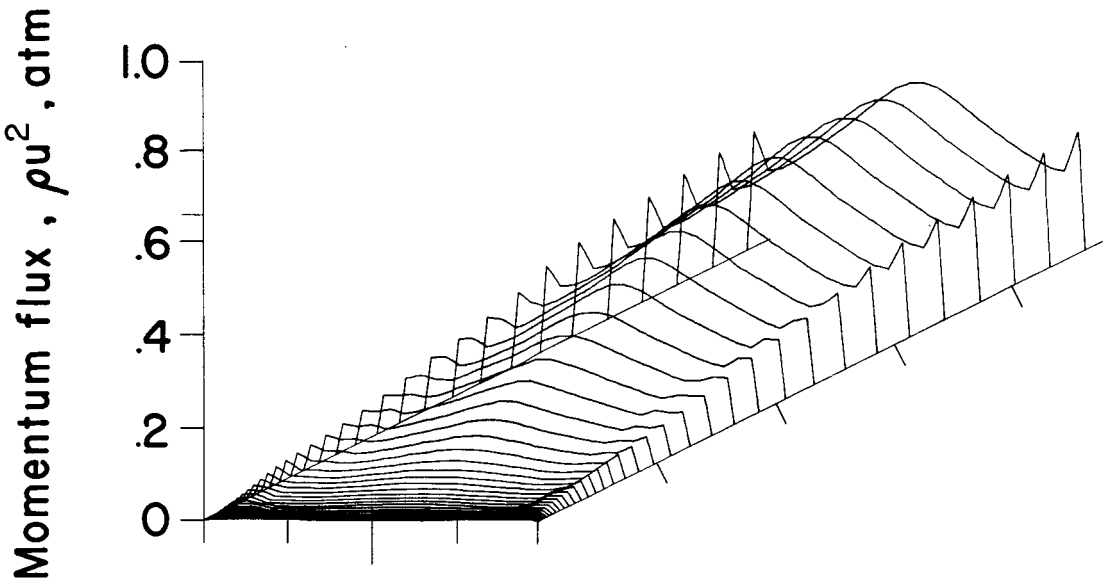

(d) Variation of momentum flux with length and radius.

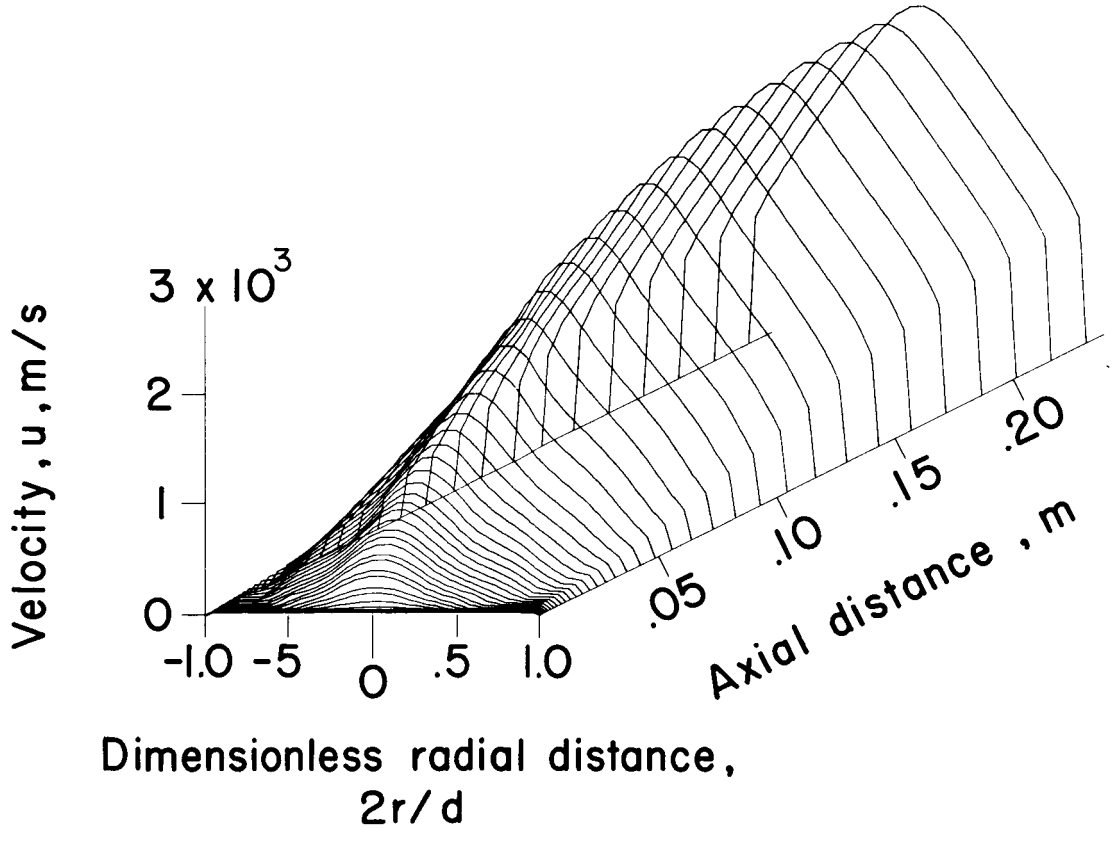

(e) Variation of velocity with length and radius.

Fig. 8.- Concluded.

NATIONAL AERONAUTICS AND SPACE ADMINISTRATION
AMES RESEARCH CENTER, MOFFETT FIELD, CALIFORNIA

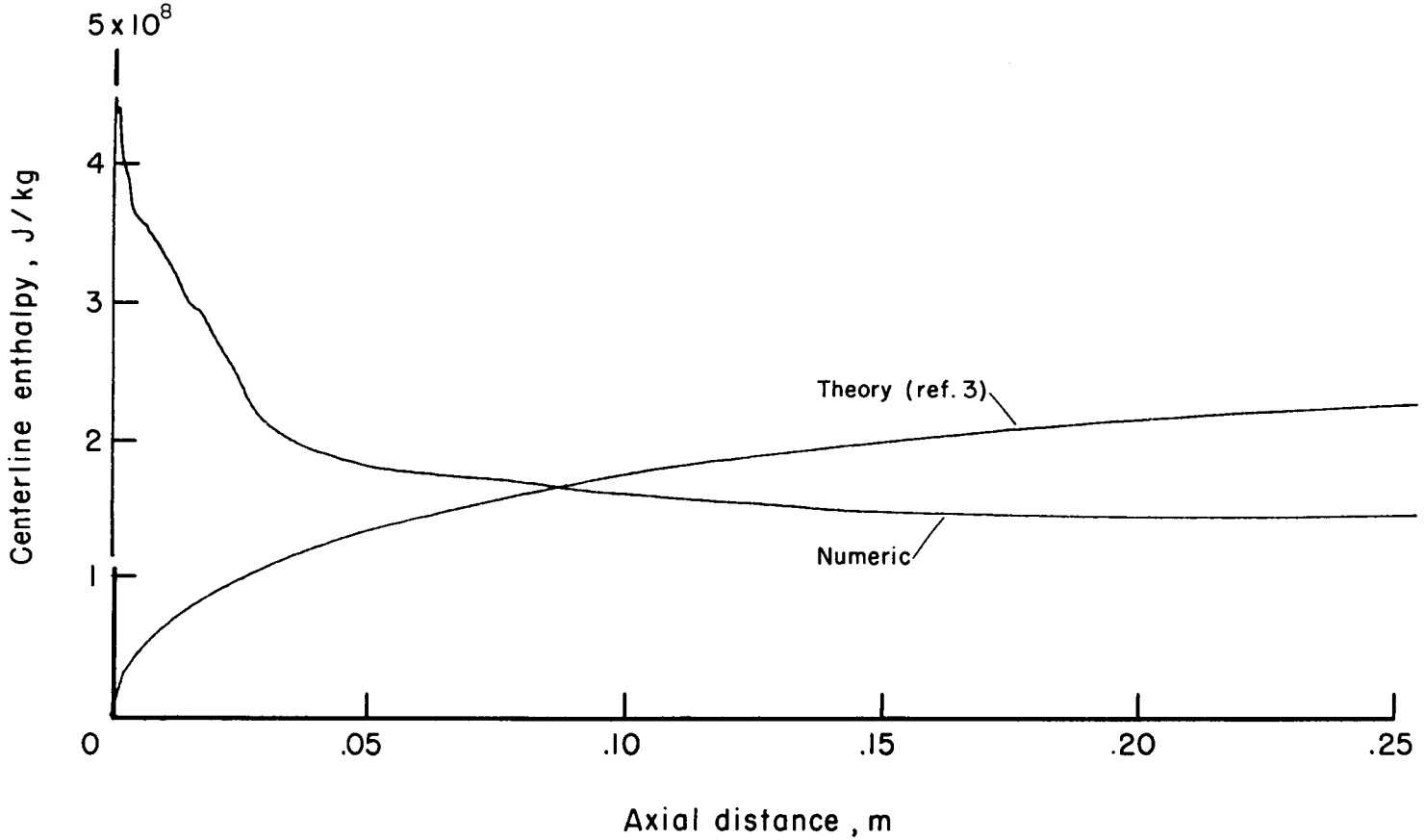

(a) Variation of center-line enthalpy with axial distance.

Fig. 9.- Comparison of numerical calculations and analytical calculations with various experimental measurements at a current of 770 A and air flow of 0.0016 kg/sec.

NATIONAL AERONAUTICS AND SPACE ADMINISTRATION
AMES RESEARCH CENTER, MOFFETT FIELD, CALIFORNIA

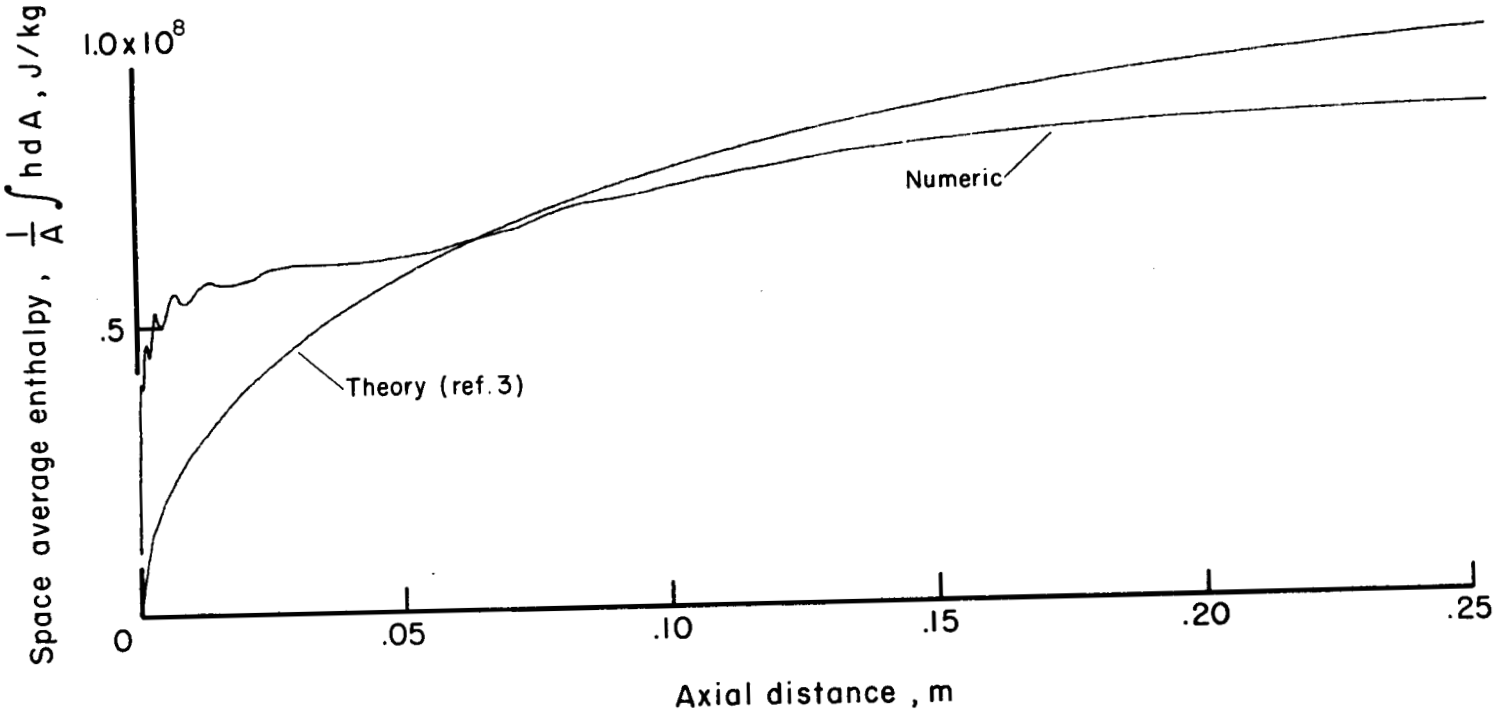

(b) Variation of space average enthalpy with axial distance.

Fig. 9.- Continued.

NATIONAL AERONAUTICS AND SPACE ADMINISTRATION
AMES RESEARCH CENTER, MOFFETT FIELD, CALIFORNIA

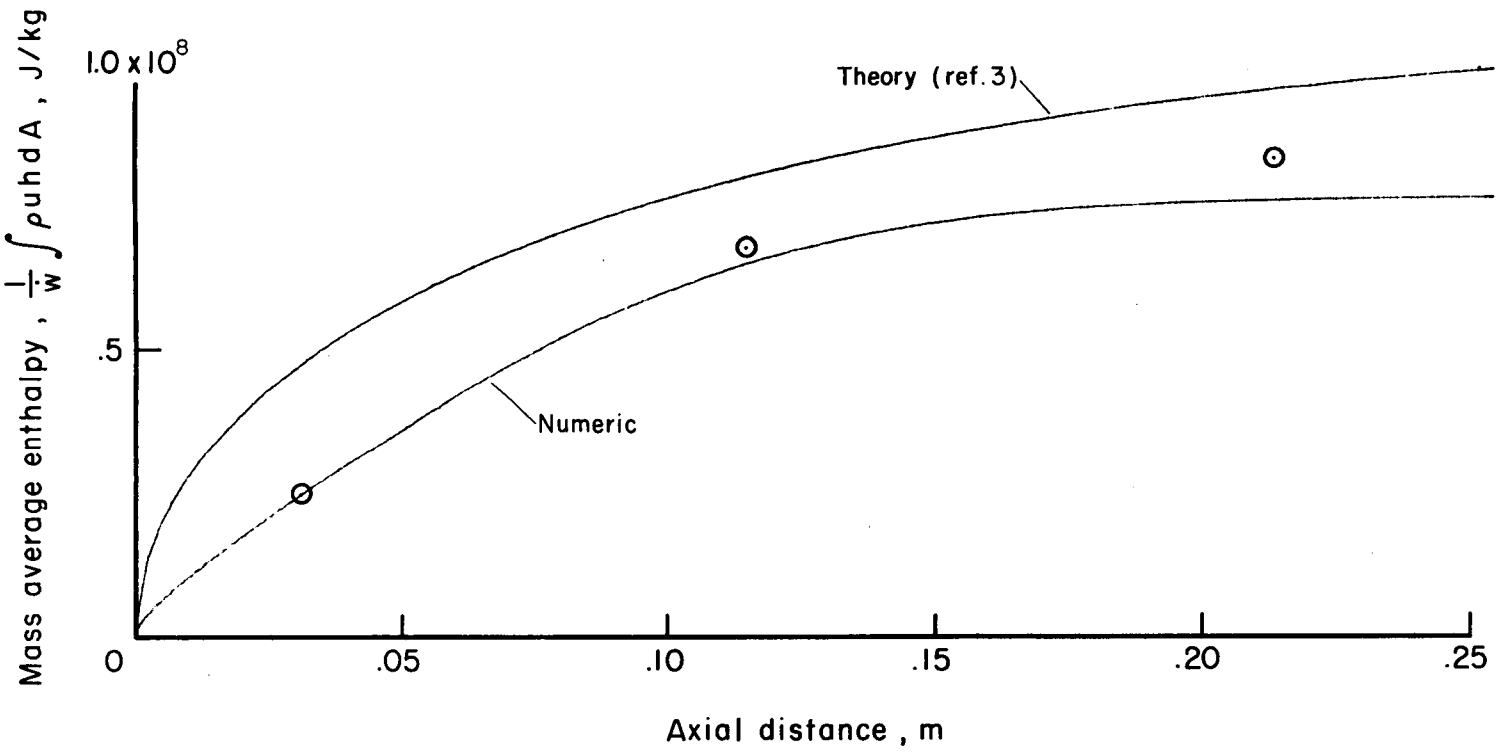

(c) Variation of mass average enthalpy with axial distance.

Fig. 9.- Continued.

NATIONAL AERONAUTICS AND SPACE ADMINISTRATION
AMES RESEARCH CENTER, MOFFETT FIELD, CALIFORNIA

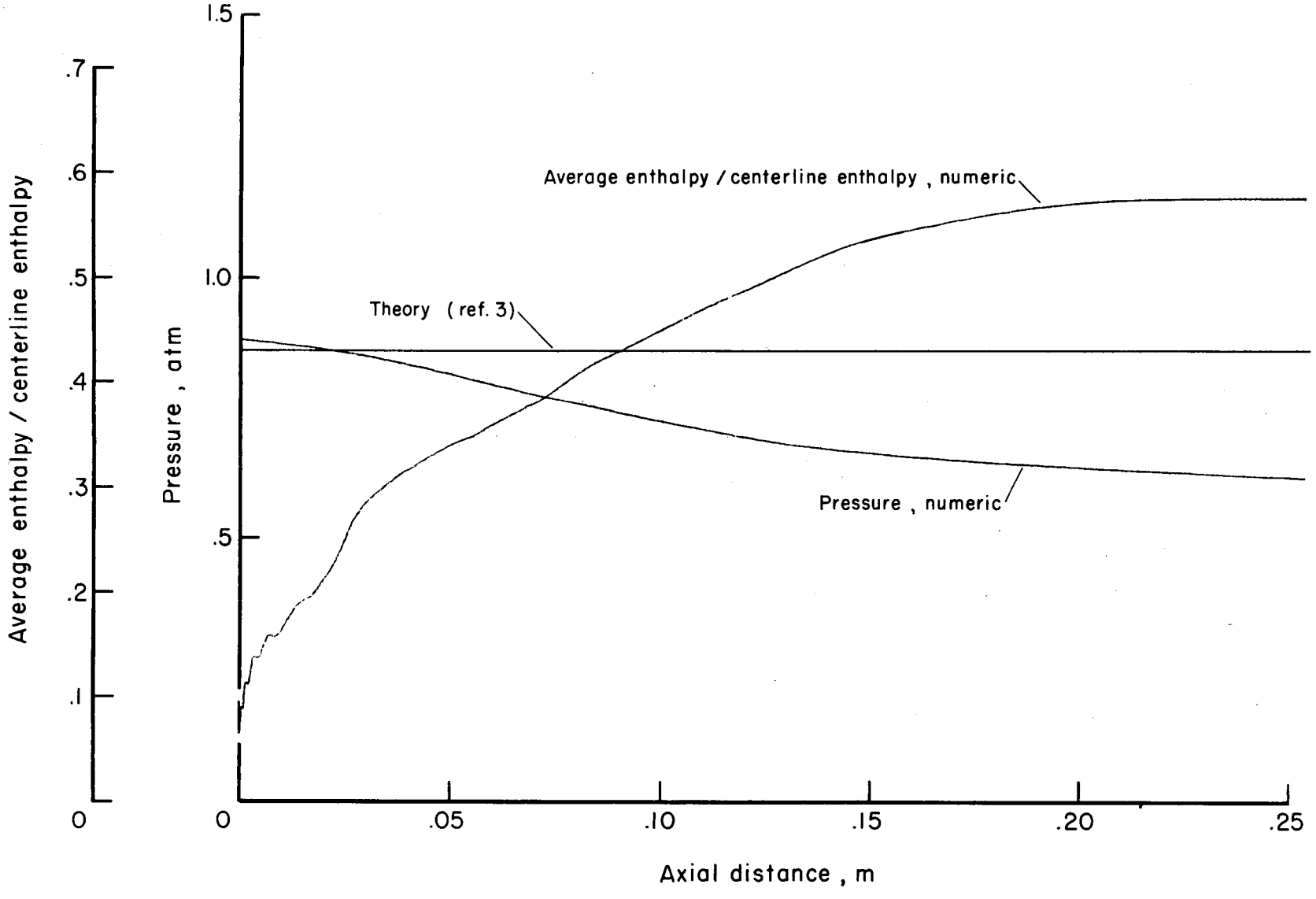

(d) Variation of pressure and ratio of average enthalpy to center-line enthalpy with axial distance.

Fig. 9.- Continued.

NATIONAL AERONAUTICS AND SPACE ADMINISTRATION
AMES RESEARCH CENTER, MOFFETT FIELD, CALIFORNIA

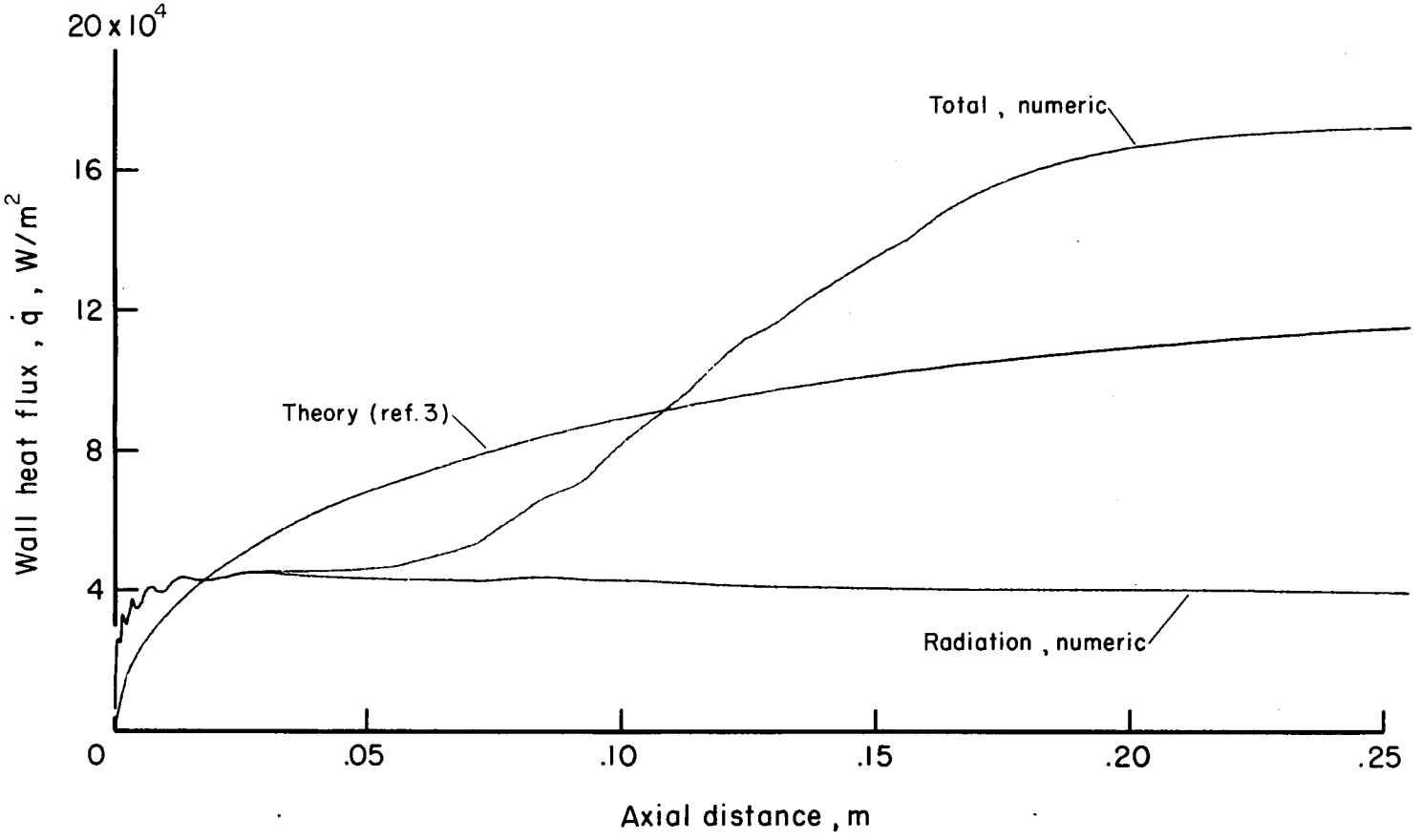

(e) Variation of wall heat flux with axial distance.

Fig. 9.- Continued.

NATIONAL AERONAUTICS AND SPACE ADMINISTRATION
AMES RESEARCH CENTER, MOFFETT FIELD, CALIFORNIA

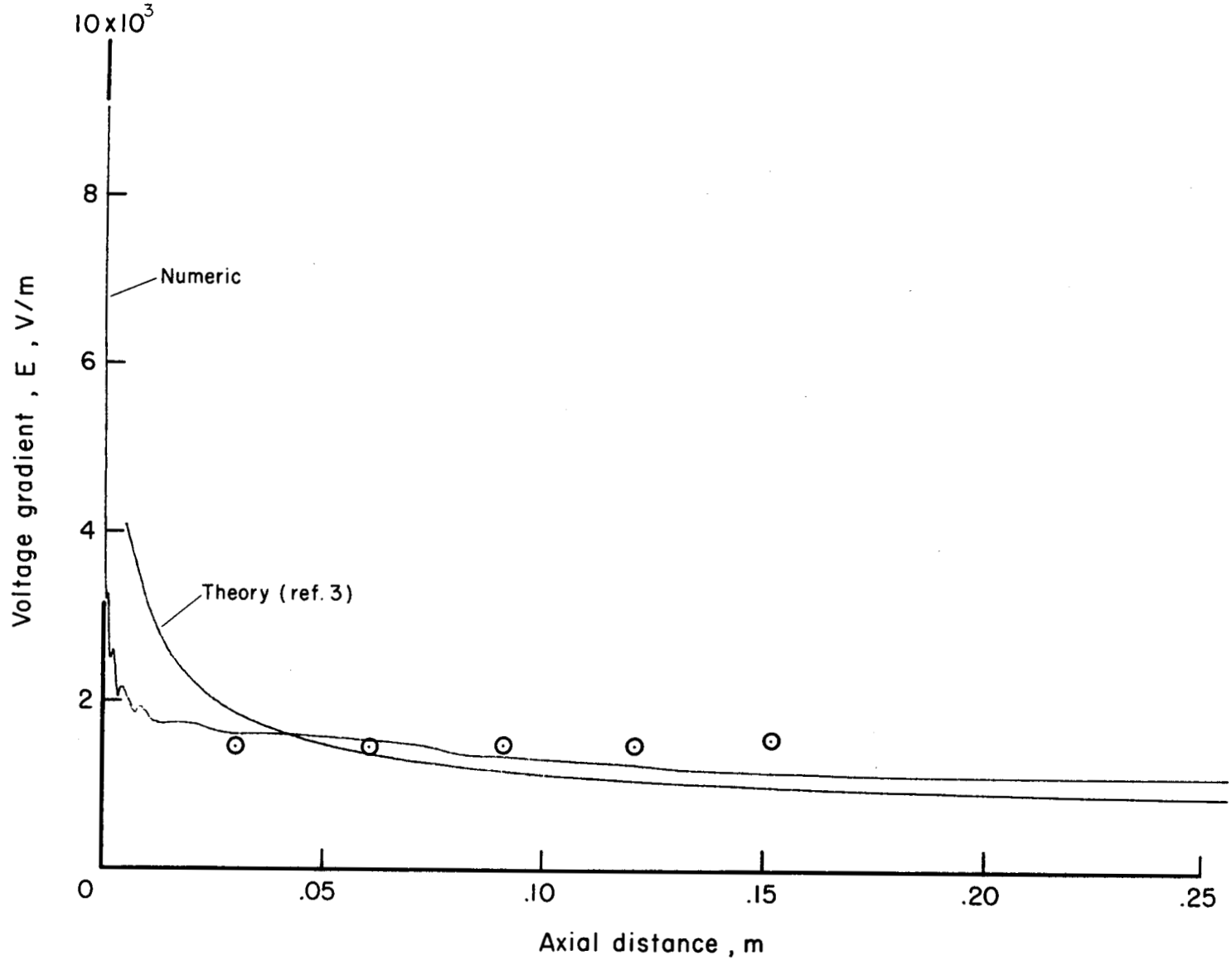

(f) Variation of voltage gradient with axial distance.

Fig. 9.- Concluded.

NATIONAL AERONAUTICS AND SPACE ADMINISTRATION
AMES RESEARCH CENTER, MOFFETT FIELD, CALIFORNIA

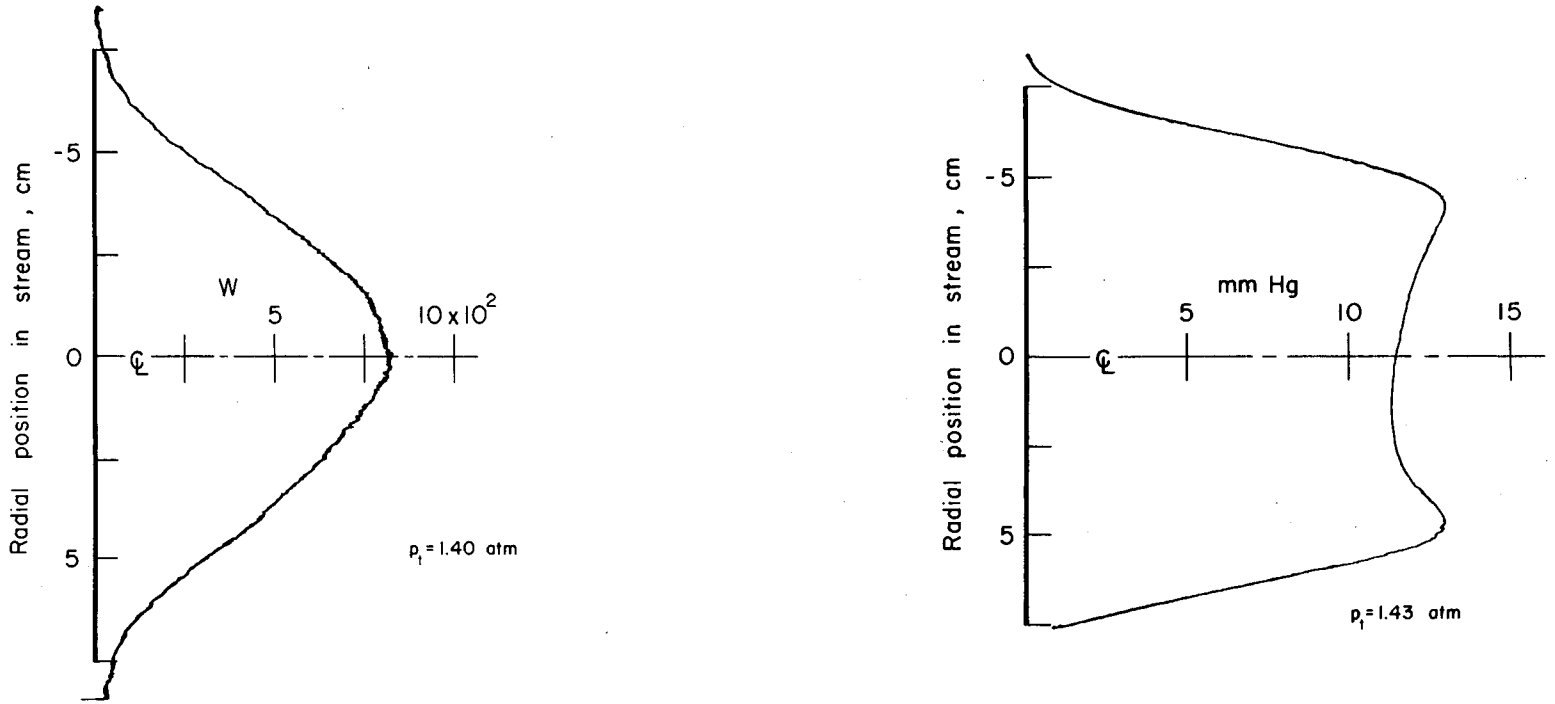

(a) Heat flux and impact pressure profiles at power input of 215 kw.

Fig. 10.- Measured radial distributions of heat flux and impact pressure at nozzle exit for air flow of 0.005 kg/sec.

NATIONAL AERONAUTICS AND SPACE ADMINISTRATION
AMES RESEARCH CENTER, MOFFETT FIELD, CALIFORNIA

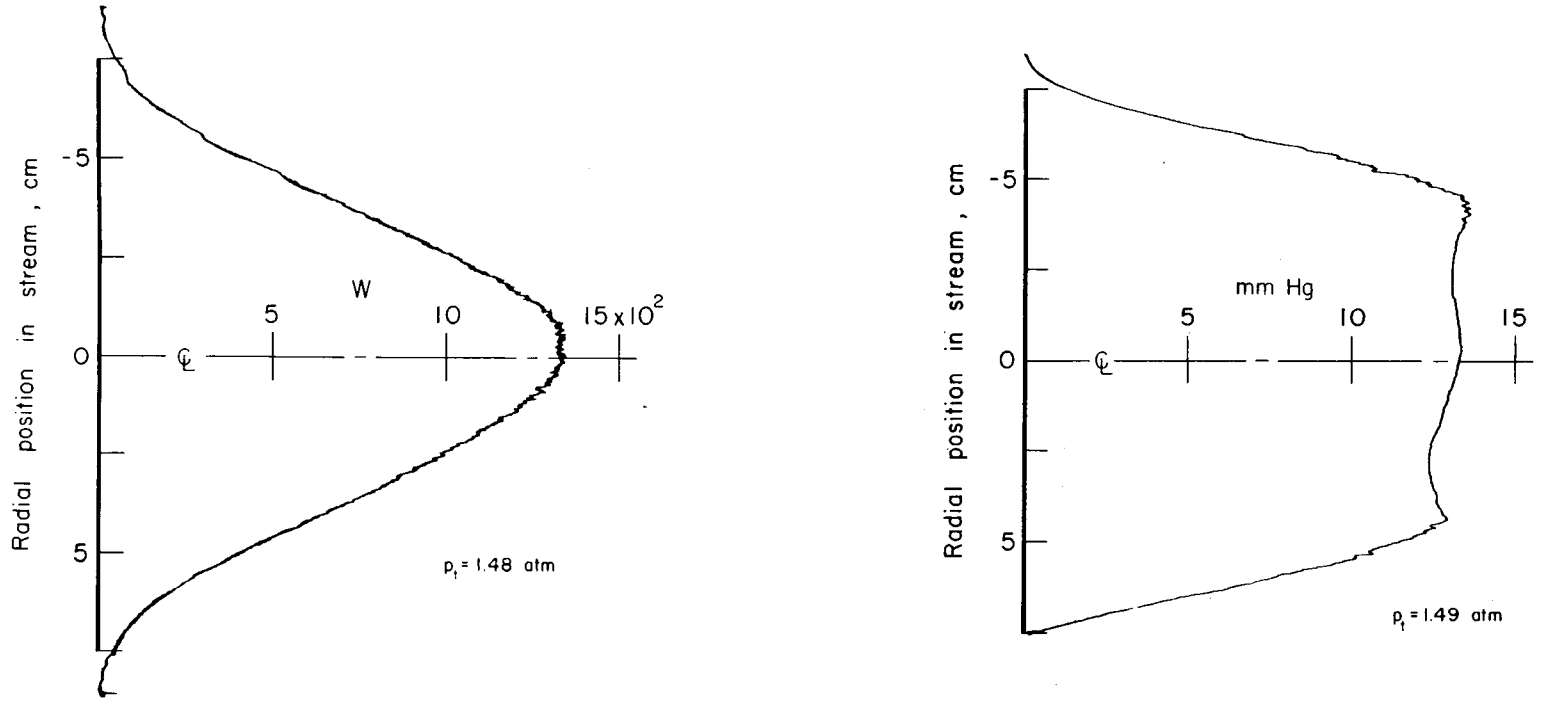

(b) Heat flux and impact pressure profiles at power input of 285 kw.

Fig. 10.- Continued.

NATIONAL AERONAUTICS AND SPACE ADMINISTRATION
AMES RESEARCH CENTER, MOFFETT FIELD, CALIFORNIA

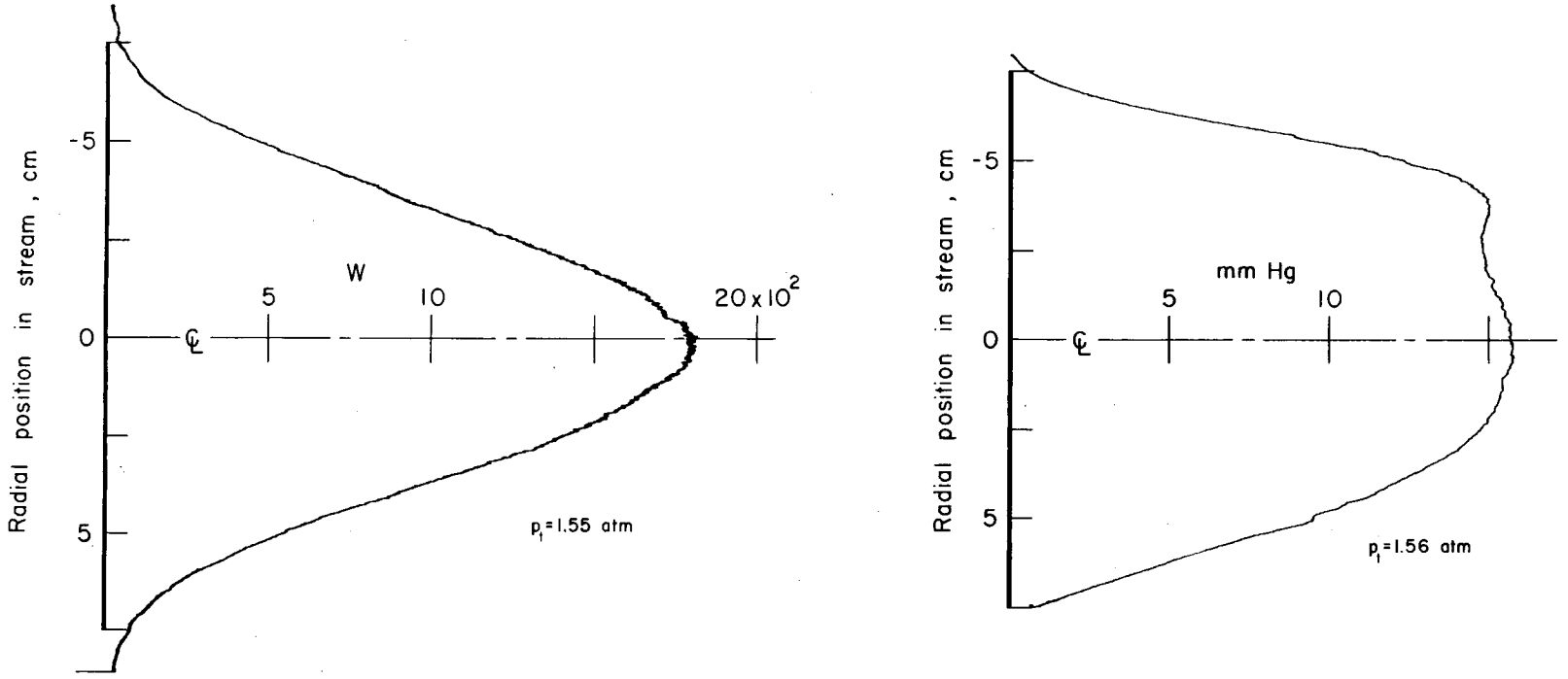

(c) Heat flux and impact pressure profiles at power input of 350 kw.

Fig. 10.- Concluded.

NATIONAL AERONAUTICS AND SPACE ADMINISTRATION
AMES RESEARCH CENTER, MOFFETT FIELD, CALIFORNIA